Realization and Detection of Nonergodic Critical Phases in an Optical Raman Lattice

Yucheng Wang,[1,2,3,†] Long Zhang,[2,3,†] Sen Niu,[2,3] Dapeng Yu,[1] and Xiong-Jun Liu[2,3,4,1,*]
[1]*Shenzhen Institute for Quantum Science and Engineering, and Department of Physics, Southern University of Science and Technology, Shenzhen 518055, China*
[2]*International Center for Quantum Materials, School of Physics, Peking University, Beijing 100871, China*
[3]*Collaborative Innovation Center of Quantum Matter, Beijing 100871, China*
[4]*CAS Center for Excellence in Topological Quantum Computation, University of Chinese Academy of Sciences, Beijing 100190, China*

(Received 14 February 2020; accepted 21 July 2020; published 12 August 2020)

The critical phases, being delocalized but nonergodic, are fundamental phases different from both the many-body localization and ergodic extended quantum phases, and have so far not been realized in experiment. Here we propose an incommensurate topological insulating model of AIII symmetry class to realize such critical phases through an optical Raman lattice scheme, which possesses a one-dimensional (1D) spin-orbit coupling and an incommensurate Zeeman potential. We show the existence of both noninteracting and many-body critical phases, which can coexist with the topological phase, and show that the critical-localization transition coincides with the topological phase boundary in noninteracting regime. The dynamical detection of the critical phases is proposed and studied in detail based on the available experimental techniques. Finally, we demonstrate how the proposed critical phases can be achieved within the current ultracold atom experiments. This work paves the way to observe the novel critical phases.

DOI: 10.1103/PhysRevLett.125.073204

Introduction.—Anderson localization (AL) is a highly explored fundamental quantum phenomenon in condensed matter physics [1], showing the disorder-induced localization of electronic wave functions. Recent experiments have observed AL in an one-dimensional (1D) optical lattice with random disorder [2] and in incommensurate quasiperiodic optical lattice [3,4]. The 1D disordered or incommensurate quantum systems may stay localized when interactions are considered, leading to the many-body localization (MBL), which is an ergodicity-breaking phase. The existence of MBL phase has been well established in both theory [5–11] and experiment [12–16].

Between the localization and ergodic extended phases, a third type of fundamental phases, called critical phases, can exist without or with interactions, with the latter case leading to the many-body critical (MBC) phase which is an extended but nonthermal quantum many-body state [17]. Critical phases are important in understanding the transitions from localization or MBL to extended phases, and exhibit various interesting features, including the critical spectral statistics [18–20], multifractal behavior of wave functions [21–23], and dynamical evolutions [24–26]. The 1D and 2D systems are localized at infinitesimal random disorder regime [27], hence may only possibly host the critical phases in quasiperiodic cases. So far only few theoretical models may host critical phases, including the 1D extended Aubry-André-Harper model [28] with incommensurate off-diagonal hopping and on site potential [29–31] which further gives MBC phase in the interacting regime [17], and the 1D quasiperiodic chain of p-wave superconductor [32–34]. However, these models are not realistic in experiment. Further, the experimental diagnostic for detecting the critical phases is lacking [16].

Recently, the optical Raman lattice has been actively studied for realizing spin-orbit (SO) coupling and topological phases with ultracold atoms in both theory [35–44] and experiment [45–49]. In this Letter, we propose for the first time an incommensurate optical Raman lattice scheme to realize the nonergodic critical phases, which respect chiral symmetry and belong to 1D AIII symmetry class. This scheme adopts an incommensurate Zeeman potential that can drive the 1D chiral topological system into critical phases or localization phases depending on its strength. The phase diagram with a broad region of critical phases is obtained, and the detection is further proposed and studied in detail. This proposal is of high feasibility and can be immediately achieved based on the current experiments.

Model.—We consider a 1D SO coupled atomic quantum gas in optical lattice with an incommensurate Zeeman potential. The Hamiltonian is

$$H = H_0 + U\sum_j n_{j\uparrow}n_{j\downarrow}, \tag{1}$$

where U denotes the Hubbard interaction, the particle number operator $n_{i,\sigma} = c^\dagger_{i,\sigma}c_{i,\sigma}$ at ith site, with $c_{i,\sigma}$ the annihilation operator at spin $\sigma = \uparrow, \downarrow$, and

$$H_0 = -t_0\sum_{\langle i,j\rangle}(c^\dagger_{i,\uparrow}c_{j,\uparrow} - c^\dagger_{i,\downarrow}c_{j,\downarrow}) + \sum_i \delta_i(n_{i,\uparrow} - n_{i,\downarrow}) + \sum_i [t_{\rm so}(c^\dagger_{i,\uparrow}c_{i+1,\downarrow} - c^\dagger_{i,\uparrow}c_{i-1,\downarrow}) + \text{H.c.}]. \quad (2)$$

Here t_0 ($t_{\rm so}$) represents the spin-conserved (spin-flip) hopping strength between neighboring sites. The Zeeman splitting $\delta_i = M_z\cos(2\pi\beta i + \phi)$ with an irrational number β and a phase offset ϕ denotes the spin-dependent incommensurate potential with strength M_z, whose realization will be given later. The Hamiltonian H_0 respecting chiral symmetry defined by σ_y in spin space renders an incommensurate optical Raman lattice model, whose counterpart with a constant uniform Zeeman potential $\delta_i = m_z$ can give rise to the 1D AIII class topological insulator [35,40,47,50]. For convenience, we set $t_0 = 1$ as the unit energy. The optimal factor $\beta = (\sqrt{5}-1)/2$ is approached by $\beta = \lim_{n\to\infty}(F_{n-1}/F_n)$, where the Fibonacci numbers $F_{n+1} = F_{n-1} + F_n$, with $F_{0,1} = 1$ [51]. In noninteracting cases, $\beta = F_{n-1}/F_n$ is taken for the system size $L = F_n$ to ensure a periodic boundary condition.

Noninteracting critical phase.—We first study the noninteracting regime with $U = 0$, where the model can be diagonalized exactly. In this regime, the phase diagram can be determined by the fractal dimension (FD), which for an arbitrary mth eigenstate $|\psi_m\rangle = \sum_j^L[u_{m,j}c^\dagger_{j,\uparrow} + v_{m,j}c^\dagger_{j,\downarrow}]|vac\rangle$ is defined as $\eta = -\lim_{L\to\infty}\ln(\text{IPR})/\ln L$, with the inverse participation ratio (IPR) being $\text{IPR}(m) = \sum_j(u^4_{m,j} + v^4_{m,j})$. It is known that $\eta \to 1$ (0) for the noninteracting extended (localized) states, while $0 < \eta < 1$ for critical states. To characterize the phases we define the mean IPR over all eigenstates: $\text{MIPR} = (2L)^{-1}\sum_{m=1}^{2L}\text{IPR}(m)$, and the mean FD $\bar{\eta} = -\lim_{L\to\infty}\ln\text{MIPR}/\ln L$. In Fig. 1(a), we display $\bar{\eta}$ as a function of M_z and $t_{\rm so}$, which clearly characterize three distinct phases, i.e., extended (I, with $\bar{\eta}\to 1$), critical (II, with $0 < \bar{\eta} < 1$), and localized (III, with $\bar{\eta}\to 0$) phases. The phase boundaries is precisely determined from a finite-size scaling analysis [52]:

$$M_z^c = \begin{cases} 2|t_0 - t_{\rm so}|, & \text{between I and II,} \\ 2(t_0 + t_{\rm so}), & \text{between II and III.} \end{cases} \quad (3)$$

The FD η also shows that all eigenstates in region II are critical [Fig. 1(b)]. Note that the critical-localized phase transition coincides the topological phase boundary. The in-gap edge states exist in the critical phase, rendering a 1D AIII class topological critical phase. More details are presented in the Supplemental Material [52].

The realized phases can be experimentally detected by probing the dynamical evolution of the spatial profile or momentum distribution of quantum states. We take the initial wave function to be a Gaussian wave packet with

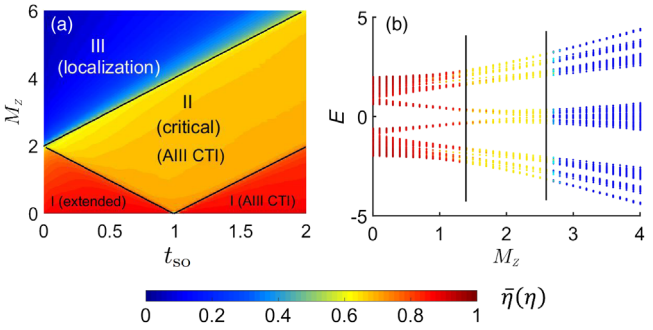

FIG. 1. (a) The mean FD $\bar{\eta}$ with $L = F_{14} = 610$ as a function of M_z and $t_{\rm so}$. Regions I, II, and III correspond to extended, critical, and localization phases, respectively, and the solid lines represent the boundaries of different phases. In both extended and critical phases, the system is a 1D AIII incommensurate chiral topological insulator (denoted as CTI). (b) The FD η of all eigenstates for different M_z with $L = 610$ and $t_{\rm so} = 0.3$. The two solid lines represent the phase boundaries $M_z^c = 1.4$ and 2.6. Here we set $\phi = 0$.

half width a at say spin-up and centered at the site j_0, i.e., $\psi_j(t=0) = (\sqrt{\pi}a)^{-1/2}e^{-(j-j_0)^2/2a^2}\binom{1}{0}$, and characterize the expansion dynamics of the wave packet by using the mean square displacement

$$W(t) = \left[\sum_{j,\sigma=\uparrow,\downarrow}(j-j_0)^2\langle n_{j,\sigma}(t)\rangle\right]^{1/2}, \quad (4)$$

which is a measurement of the width of the wave packet. The quantity $W(t)$ can be detected by direct *in situ* imaging with both Bose [2,3] and Fermi [4,57] systems. Figure 2(a) displays how W evolves with time (in units of $\hbar/t_0$) for different M_z with $a = 5$. We observe that for the extended phase obtained in the relatively small M_z, W reaches a large and stable value in a fairly short time, while for large M_z, W remains very small all the time, signifying the localization of the wave packet. In comparison, for the critical phase, W grows gradually and slowly, different from both extended and localization regimes. The different behaviors can be quantified as

$$W(t) \sim t^\kappa, \quad (5)$$

where the dynamical index κ can be shown to take $\kappa = 1$, $\kappa = 0$, and $\kappa \approx 1/2$ corresponding to the extended, localized, and critical phases, respectively [52]. A related observable to distinguish the phases is $\bar{W} = (1/N_t)\sum_{m=1}^{N_t}W(m\Delta T)$, which reflects the mean width of the wave packet over a long period of time. Here the sum is taken over a stroboscopic time evolution in steps of ΔT. The results are shown in Fig. 2(b) for different a with $\Delta T = 50$ and $N_t = 40$. The two points where $\bar{W}$ decreases rapidly indicate the locations of phase boundaries, which are independent of the width a, and an approximate plateau in between marks the critical phase.

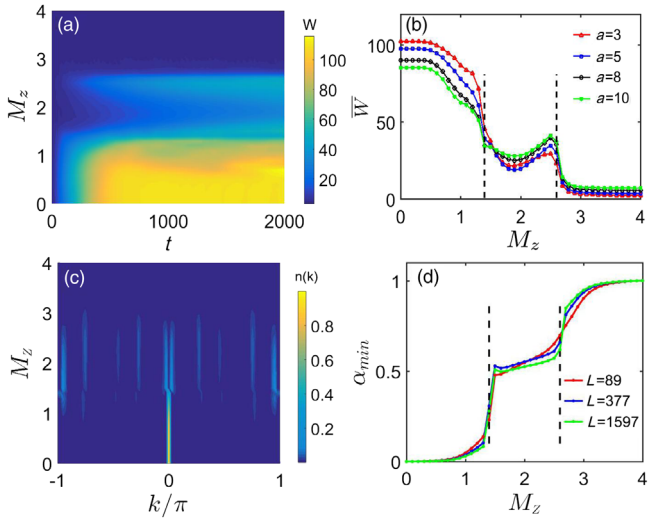

FIG. 2. (a) W as a function of M_z and time t with initial half width $a = 5$ and lattice size $L = F_{13} = 377$. (b) $\bar{W}$ versus M_z for different a with fixed size $L = 377$. (c) Ground state momentum distribution $n(k)$ for different M_z with $L = F_{10} = 89$. (d) The minimal index $\alpha_{\min}$ versus M_z for $L = 89$, 377 and $L = F_{16} = 1597$. Here we take $t_{so} = 0.3$ and $\phi = 0$.

The wave packet width a has a clear influence on the expansion speed, and should be properly prepared for experimental detection (see the experimental realization part and the Supplemental Material [52]).

The critical phase can also be detected by measuring the momentum distribution, which is applicable to the system for ultracold bosons, given by

$$n(k) = \frac{1}{L}\sum_{i,j=1}^{L} e^{-ik(i-j)}(\rho_{ij}^{\uparrow} + \rho_{ij}^{\downarrow}). \tag{6}$$

Here $\rho_{ij}^{\sigma} = \langle\psi_m|c_{i,\sigma}^{\dagger}c_{j,\sigma}|\psi_m\rangle$ are the single-particle density matrices with respect to the eigenstate $|\psi_m\rangle$. The momentum distribution exhibits localized, multifractal, and extended features in different regions [see Fig. 2(c)]. Quantitatively, we introduce the fractal index $\alpha(k) = -\ln n(k)/\ln L$, and examine the minimal index $\alpha_{\min}$, which characterizes the distribution peak $n_{\max}$. When $L \to \infty$, we see $\alpha_{\min} = 0$, $\alpha_{\min} = 1$, and $0 < \alpha_{\min} < 1$ for the extended, localization, and critical phases, respectively [Fig. 2(d)]. The experimental diagnostics for different phases are summarized in Table I.

Many-body critical phase.—When the Hubbard interaction is included, the critical phase in the noninteracting regime may enter a new fundamental many-body state, namely, the MBC phase which is extended but not thermalizable [17]. We here propose to study the universal quench dynamics in the interacting regime, which on one hand confirms the existence of the MBC, and on the other hand provides experimental detection of the phase. For convenience, we take $U = 1$ and consider the quarter filling

TABLE I. The observables $\bar{W}$, κ, and $\alpha_{\min}$ ($L \to \infty$) in different phases, where r (k) implies the corresponding quantity is measured in real (momentum) space, and B(F) indicates it is measurable in ultracold Bose (Fermi) atoms.

Phases	Extended	Critical	Localized
$\kappa(r)$ (B, F)	1	≈ 0.5	0
$\bar{W}(r)$ (B, F)	Maximum	Middle plateau	Minimum
$\alpha_{\min}(k)$ (B)	0	$\in (0, 1)$	1

with the initial state $|\Psi(0)\rangle = |\uparrow 0 \uparrow 0 \uparrow 0 \uparrow \cdots\rangle$, namely, $N = L/2$, which can be created by applying a superlattice initially [12]. Fixing the initial state facilitates the further measurement, while our main results are independent of the specific initial configuration.

We study the return probability of the many-body state under the evolution of the total Hamiltonian H, given by $P(t) = |\langle\Psi(0)|\Psi(t)\rangle|^2$, with $|\Psi(t)\rangle$ the state after evolution time t. This observable has been measured in interacting many-body systems to observe the dynamical quantum phase transition [58,59]. By using $|\Psi(t)\rangle = \sum_n e^{-iE_n t}|\varphi_n\rangle\langle\varphi_n|\Psi(0)\rangle$, where $|\varphi_n\rangle$ are many-body eigenstates with eigenvalues E_n, one can obtain the long-time average of the return probability

$$\bar{P} = \lim_{T\to\infty}\frac{1}{T}\int_0^T dtP(t) = \sum_n |\langle\varphi_n|\Psi(0)\rangle|^4, \tag{7}$$

which resembles the IPR with the leading term $\bar{P} \sim D_H^{-\eta}$. Here D_H is the Hilbert space size and $\eta \to 1$, $0 < \eta < 1$ and $\eta \to 0$ for the ergodic, MBC, and MBL phases, respectively [17]. This result tells that the MBL (ergodic extended) phase preserves (loses) the local quantum information of initial state after a long time evolution [61]. The critical phase loses local information with a lower speed. To further distinguish MBC from ergodic extended phase, we consider the density imbalance

$$I = \frac{N_{\text{odd}} - N_{\text{even}}}{N_{\text{odd}} + N_{\text{even}}}, \tag{8}$$

where N_{odd} (N_{even}) denotes the atom number on odd (even) sites. The imbalance I can be measured using the superlattice band-mapping technique [12]. The long-time average of particle number at site j can be predicted by a microcanonical ensemble analysis if the system is ergodic [62], i.e., $\bar{n}_j = \lim_{T\to\infty}(1/T)\int_0^T dtn_j(t) = \langle n_j\rangle_{\text{microcan}}(E_0)$, where E_0 is the energy of the initial state. The particle distribution of $|\Psi(t)\rangle$ for large t is then independent of the initial distribution, hence the final distribution is uniform, giving $I = 0$. In contrast, for the nonthermal critical phase, I remains a finite value after a long time evolution. Therefore, the MBC phase can be distinguished from the other two through a combined measurement of P and I.

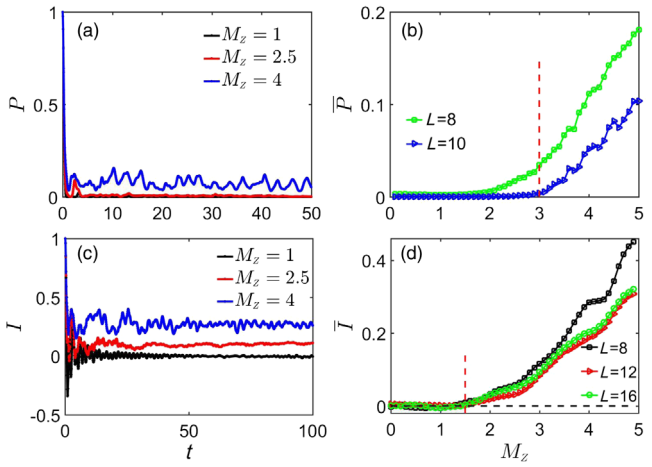

FIG. 3. Time evolution of (a) the return probability with $L = 10$ and (c) the density imbalance I with $L = 16$ for $M_z = 1$, 2.5, 4, respectively. (b) $\bar{P}$ obtained from Eq. (7) versus M_z with $L = 8$ or 10. The red dashed line denotes $M_z = 3$. (d) $\bar{I}$ as a function of M_z for different L. Red and black dashed lines correspond to $M_z = 1.5$ and $\bar{I} = 0$, respectively. Here we fix $t_{so} = 0.3$ and use both the exact diagonalization method (for $L = 8$, 10) and time-density matrix renormalization group method (for $L = 12$, 16). To reduce the fluctuation, we take an average over 10 realizations with different initial phase ϕ.

Figure 3(a) shows the behavior of the return probability P, which quickly decays to zero when $M_z = 1$ or 2.5, signifying that the phases are extended. In contrast, P maintains a nonvanishing value during the evolution at $M_z = 4$, indicating that the system enters the MBL phase. The long-time average $\bar{P}$ is displayed as a function of M_z in Fig. 3(b). One can see that $\bar{P}$ increases from zero to nonzero around the point $M_z = 3$ for $L = 10$. However, for $L = 8$, the transition point moves to the regime $M_z < 3$. We attributes it to the finite-size effect [63]. Hence we can conclude that when $L \to \infty$, the critical point of the delocalization-localization transition is a bit larger than $M_z = 3$. We then examine the density imbalance I, as shown in Fig. 3(c). It demonstrates that the system is ergodic when $M_z = 1$, but nonergodic when $M_z = 2.5$ or 4. Combing Fig. 3(a), we find the system to be in the MBC phase for $M_z = 2.5$. Figure 3(d) shows the long-time average imbalance $\bar{I}$, which is numerically calculated by using $\bar{I} = (2/T)\int_{T/2}^{T} dtI(t)$ with $T = 100$, and it approximates the stable value of I after long time evolution. We see that the ergodicity breaking transition occurs near $M_z = 1.5$, insensitive to system size. The combined measurements show that the approximate region with $M_z \in (1.5, 3)$ belongs to the extended and nonthermal MBC phase.

Proposal for experimental realization.—Finally we propose a highly feasible experimental setup to realize the Hamiltonian (1) based on optical Raman lattices [35,40,47]. As depicted in Fig. 4(a), a standing-wave beam $\mathbf{E}_1$ (red) with x polarization and a plane wave $\mathbf{E}_3$ (green) with z polarization are applied to generate a spin-independent main lattice $V_1(z)$ and a Raman coupling potential $\mathcal{M}(z)$ simultaneously. The former induces the spin-conserved hopping and the latter produces the spin-flip hopping [Fig. 4(b)]. In addition, another standing wave $\mathbf{E}_2$ (blue), formed by two counter-propagating lights with mutually perpendicular polarization, is used to produce a spin-dependent lattice $V_2(z)$ [40,64], which provides a secondary incommensurate Zeeman potential.

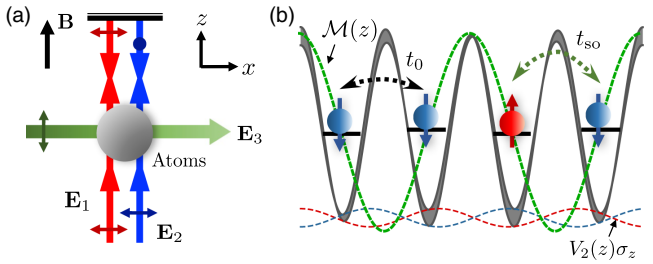

FIG. 4. Experimental realization in cold atoms. (a) Experimental setup. A standing wave $\mathbf{E}_1$ with x polarization generates the spin-independent primary lattice. Another beam $\mathbf{E}_2$, formed by two counterpropagating lights with mutually perpendicular polarization, gives a spin-dependent incommensurate lattice. A plane wave $\mathbf{E}_3$ is applied to form a Raman coupling potential with one component of $\mathbf{E}_1$. (b) Spin-conserved (t_0) and -flipped (t_{so}) hoppings are induced by the primary lattice and Raman potential, respectively. The secondary lattice provides an incommensurate spin-dependent offset.

With the bias field $\mathbf{B}$ applied along the z direction, the standing wave $\mathbf{E}_1$ with x polarization can be written as $\mathbf{E}_1 = \hat{e}_+ E_{1+}\cos(k_1 z) + \hat{e}_- E_{1-}\cos(k_1 z)$ with $E_{1\pm}$ being the amplitudes. For alkali-metal atoms, the optical lattice potential is spin independent, which reads $V_1(z) = V_p \cos^2(k_1 z)$ with the depth $V_p \propto (E_{1+}^2 + E_{1-}^2)/\Delta$, and creates a tight-binding primary lattice. Here Δ denotes the coupling detuning. Having the plane-wave field $\mathbf{E}_3 = \hat{e}_z E_3 e^{ik_3 x}$, one Raman potential $\mathcal{M}(z) = M_R \cos(k_1 z)$, with $M_R \propto E_{1-}E_3/\Delta$, can be generated by E_3 and the E_{1-} component. The Raman and lattice potentials satisfy a relative antisymmetry, which ensures a spin-flipped hopping along the z direction [35,50]. The other standing-wave field reads $\mathbf{E}_2 = \hat{e}_+ E_{2+}\cos(k_2 z) + \hat{e}_- E_{2-}\sin(k_2 z)$ gives the secondary lattice $V_2(z)\sigma_z = (V_s/2)\cos(2k_2 z)\sigma_z$, with $V_s \propto (E_{2+}^2 - E_{2-}^2)/\Delta$, which provides a weak spin-dependent energy offset, with the irrational number $\beta = k_2/k_1$ [52]. The realization only necessitates a weak incommensurate lattice, and the hopping parameters are determined by the primary lattice and Raman potentials [Fig. 4(b)]. The model parameters can be tuned independently.

Here we take ^{40}K fermions as an example, while the realization is also applicable to bosons, such as ^{87}Rb atoms. For ^{40}K, we choose $|\uparrow\rangle = |F = 7/2, m_F = +7/2\rangle$, and $|\downarrow\rangle = |9/2, +9/2\rangle$ to construct the spin-1/2 system, and set the wavelengths of $\mathbf{E}_{1,2}$ to be $\lambda_1 = 768$ nm and $\lambda_2 = 798$ nm, which yields $\beta \approx 0.9624$ if the two beams are parallel. We then have $V_s/V_p \sim E_2^2/162E_1^2$ and $M_R/V_p \sim E_3/E_1$ [52]. One can tune the lattice and Raman potentials

freely by the laser intensity. For example, the settings $V_p = 4.2E_r$ and $M_R = 0.4E_r$ with $E_r \equiv \hbar^2 k_1^2/2m$ give $t_{so} \simeq 0.3t_0$; the noninteracting critical phase, which corresponds to the parameter region $1.4t_0 < |M_z| < 2.6t_0$, can be realized by tuning V_s in the range from $0.43E_r$ to $0.80E_r$ [52]. The critical phase can be detected by monitoring the atom cloud expansion and measuring the evolution of the observable $W(t)$, which can be initiated by suddenly switching off the external harmonic trap that initially confines the atoms. With the above parameters the ^{40}K ultracold system has a relatively short lifetime $\sim 2500/E_r$, which restricts the time of measurement of the expansion dynamics. A clear detection of the critical phase requires the initial atom cloud to have a small spatial half width a (≤ 10) and thus have a relatively high expansion speed, which may be achieved with a narrow and tight trapping potential. This requirement is more relaxed for ^{87}Rb bosons, whose lifetime is large $\sim 15000/E_r$. We put the numerical details of this issue in the Supplemental Material [52].

Conclusion.—We have proposed a highly feasible 1D SO coupled model with incommensurate Zeeman potential for realizing critical phases in a broad phase diagram region separating from the extended and localized phases. In the noninteracting regime, we showed that the critical phase can be detected by measuring the mean square displacement of the wave packet after a fixed time of expansion evolution in real space or measuring the momentum distributions. With interactions, we proposed two observables, i.e., the return probability of the initial state and the density imbalance, to distinguish the MBC phase from both the ergodic and MBL phases. With the study being accessible in the current experiments, this Letter opens an avenue with high experimental feasibility to explore critical phases in ultracold atoms.

We thank Immanuel Bloch for helpful comments. This work was supported by National Natural Science Foundation of China (Grants No. 11825401, No. 11761161003, and No. 11921005), the National Key R&D Program of China (Grant No. 2016YFA0301604), Guangdong Innovative and Entrepreneurial Research Team Program (Grant No. 2016ZT06D348), the Science, Technology and Innovation Commission of Shenzhen Municipality (Grant No. KYTDPT20181011104202253), and the Strategic Priority Research Program of CAS (Grant No. XDB28000000).

*Corresponding author.
xiongjunliu@pku.edu.cn
†These authors contribute equally to this work.

[1] P. W. Anderson, Absence of diffusion incertain random lattices, Phys. Rev. **109**, 1492 (1958).
[2] J. Billy, V. Josse, Z. Zuo, A. Bernard, B. Hambrecht, P. Lugan, D. Clément, L. Sanchez-Palencia, P. Bouyer, and A. Aspect, Direct observation of Anderson localization of matter waves in a controlled disorder, Nature (London) **453**, 891 (2008).
[3] G. Roati, C. D'Errico, L. Fallani, M. Fattori, C. Fort, M. Zaccanti, G. Modugno, M. Modugno, and M. Inguscio, Anderson localization of a non-interacting Bose-Einstein condensate, Nature (London) **453**, 895 (2008).
[4] H. P. Lüschen, S. Scherg, T. Kohlert, M. Schreiber, P. Bordia, X. Li, S. D. Sarma, and I. Bloch, Single-Particle Mobility Edge in a One-Dimensional Quasiperiodic Optical Lattice, Phys. Rev. Lett. **120**, 160404 (2018).
[5] A. Pal and D. A. Huse, Many-body localization phase transition, Phys. Rev. B **82**, 174411 (2010).
[6] R. Nandkishore and D. A. Huse, Many-body localization and thermalization in quantum statistical mechanics, Annu. Rev. Condens. Matter Phys. **6**, 15 (2015).
[7] E. Altman and R. Vosk, Universal dynamics and renormalization in many-body-localized systems, Annu. Rev. Condens. Matter Phys. **6**, 383 (2015).
[8] R. Vosk, D. A. Huse, and E. Altman, Theory of the Many-Body Localization Transition in One-Dimensional Systems, Phys. Rev. X **5**, 031032 (2015).
[9] X. Li, S. Ganeshan, J. H. Pixley, and S. D. Sarma, Many-Body Localization and Quantum Nonergodicit in a Model with a Single-Particle Mobility Edge, Phys. Rev. Lett. **115**, 186601 (2015).
[10] E. J. Torres-Herrera and L. F. Santos, Dynamics at the many-body localization transition, Phys. Rev. B **92**, 014208 (2015).
[11] D. A. Abanin, E. Altman, I. Bloch, and M. Serbyn, Colloquium: Many-body localization, thermalization, and entanglement, Rev. Mod. Phys. **91**, 021001 (2019).
[12] M. Schreiber, S. S. Hodgman, P. Bordia, H. P. Lüschen, M. H. Fischer, R. Vosk, E. Altman, U. Schneider, and I. Bloch, Observation of many-body localization of interacting fermions in a quasirandom optical lattice, Science **349**, 842 (2015).
[13] P. Bordia, H. P. Lüschen, S. S. Hodgman, M. Schreiber, I. Bloch, and U. Schneider, Coupling Identical One-Dimensional Many-Body Localized Systems, Phys. Rev. Lett. **116**, 140401 (2016).
[14] P. Bordia, H. Lüschen, S. Scherg, S. Gopalakrishnan, M. Knap, U. Schneider, and I. Bloch, Probing Slow Relaxation and Many-Body Localization in Two-Dimensional Quasiperiodic Systems, Phys. Rev. X **7**, 041047 (2017).
[15] H. P. Lüschen, P. Bordia, S. Scherg, F. Alet, E. Altman, U. Schneider, and I. Bloch, Observation of Slow Dynamics Near the Many-Body Localization Transition in One-Dimensional Quasiperiodic Systems, Phys. Rev. Lett. **119**, 260401 (2017).
[16] T. Kohlert, S. Scherg, X. Li, H. P. Lüschen, S. D. Sarma, I. Bloch, and M. Aidelsburger, Observation of Many-Body Localization in a One-Dimensional System with a Single-Particle Mobility Edge, Phys. Rev. Lett. **122**, 170403 (2019).
[17] Y. Wang, X.-J. Liu, and D. Yu, Many-body critical phase: Extended and nonthermal, arXiv:1910.12080.
[18] T. Geisel, R. Ketzmerick, and G. Petschel, New Class of Level Statistics in Quantum Systems with Unbounded Diffusion, Phys. Rev. Lett. **66**, 1651 (1991).

[19] K. Machida and M. Fujita, Quantum energy spectra and one-dimensional quasiperiodic systems, Phys. Rev. B **34**, 7367 (1986).
[20] C. L. Bertrand and A. M. García-García, Anomalous thouless energy and critical statistics on the metallic side of the many-body localization transition, Phys. Rev. B **94**, 144201 (2016).
[21] T. C. Halsey, M. H. Jensen, L. P. Kadanoff, I. Procaccia, and B. I. Shraiman, Fractal measures and their singularities: The characterization of strange sets, Phys. Rev. A **33**, 1141 (1986).
[22] A. D. Mirlin, Y. V. Fyodorov, A. Mildenberger, and F. Evers, Exact Relations Between Multifractal Exponents at the Anderson Transition, Phys. Rev. Lett. **97**, 046803 (2006).
[23] R. Dubertrand, I. García-Mata, B. Georgeot, O. Giraud, G. Lemarié, and J. Martin, Two Scenarios for Quantum Multifractality Breakdown, Phys. Rev. Lett. **112**, 234101 (2014).
[24] H. Hiramoto and S. Abe, Dynamics of an electron in quasiperiodic systems. II. Harper's model, J. Phys. Soc. Jpn. **57**, 1365 (1988).
[25] R. Ketzmerick, K. Kruse, S. Kraut, and T. Geisel, What Determines the Spreading of a Wave Packet?, Phys. Rev. Lett. **79**, 1959 (1997).
[26] M. Larcher, F. Dalfovo, and M. Modugno, Effects of interaction on the diffusion of atomic matter waves in one-dimensional quasiperiodic potentials, Phys. Rev. A **80**, 053606 (2009).
[27] E. Abrahams, P. W. Anderson, D. C. Licciardello, and T. V. Ramakrishnan, Scaling Theory of Localization: Absence of Quantum Diffusion in Two Dimensions, Phys. Rev. Lett. **42**, 673 (1979).
[28] S. Aubry and G. André, Analyticity breaking and Anderson localization in incommensurate lattices, Ann. Isr. Phys. Soc. **3**, 133 (1980).
[29] Y. Hatsugai and M. Kohmoto, Energy spectrum and the quantum Hall effect on the square lattice with next-nearest-neighbor hopping, Phys. Rev. B **42**, 8282 (1990).
[30] Y. Takada, K. Ino, and M. Yamanaka, Statistics of spectra for critical quantum chaos in one-dimensional quasiperiodic systems, Phys. Rev. E **70**, 066203 (2004).
[31] F. Liu, S. Ghosh, and Y. D. Chong, Localization and adiabatic pumping in a generalized Aubry-André-Harper model, Phys. Rev. B **91**, 014108 (2015).
[32] X. Cai, L.-J. Lang, S. Chen, and Y. Wang, Topological Superconductor to Anderson Localization Transition in One-Dimensional Incommensurate Lattices, Phys. Rev. Lett. **110**, 176403 (2013).
[33] J. Wang, X.-J. Liu, X. Gao, and H. Hu, Phase diagram of a non-Abelian Aubry-André-Harper model with p-wave superfluidity, Phys. Rev. B **93**, 104504 (2016).
[34] Y. Wang, Y. Wang, and S. Chen, Spectral statistics, finite-size scaling and multifractal analysis of quasiperiodic chain with p-wave pairing, Eur. Phys. J. B **89**, 254 (2016).
[35] X.-J. Liu, Z.-X. Liu, and M. Cheng, Manipulating Topological Edge Spins in a One-Dimensional Optical Lattice, Phys. Rev. Lett. **110**, 076401 (2013).
[36] X.-J. Liu, K. T. Law, and T. K. Ng, Realization of 2D Spin-Orbit Interaction and Exotic Topological Orders in Cold Atoms, Phys. Rev. Lett. **112**, 086401 (2014).
[37] J.-S. Pan, X.-J. Liu, W. Zhang, W. Yi, and G.-C. Guo, Topological Superradiant States in a Degenerate Fermi Gas, Phys. Rev. Lett. **115**, 045303 (2015).
[38] L. Lepori, I. C. Fulga, A. Trombettoni, and M. Burrello, Double Weyl points and Fermi arcs of topological semimetals in non-Abelian gauge potentials, Phys. Rev. A **94**, 053633 (2016).
[39] X. Zhou, J.-S. Pan, Z.-X. Liu, W. Zhang, W. Yi, G. Chen, and S. Jia, Symmetry-Protected Topological States for Interacting Fermions in Alkaline-Earth-Like Atoms, Phys. Rev. Lett. **119**, 185701 (2017).
[40] B.-Z. Wang, Y.-H. Lu, W. Sun, S. Chen, Y. Deng, and X.-J. Liu, Dirac-, Rashba-, and Weyl-type spin-orbit couplings: Toward experimental realization in ultracold atoms, Phys. Rev. A **97**, 011605(R) (2018).
[41] C. Zhu, L. Chen, H. Hu, X. J. Liu, and H. Pu, Spin-exchange-induced exotic superfluids in a Bose-Fermi spinor mixture, Phys. Rev. A **100**, 031602(R) (2019).
[42] H. Hu, I. I Satija, and E. Zhao, Chiral and counter-propagating Majorana fermions in a p-wave superconductor, New J. Phys. **21**, 123014 (2019).
[43] Z. Zheng, Z. Lin, D.-W. Zhang, S.-L. Zhu, and Z. D. Wang, Chiral magnetic effect in three-dimensional optical lattices, Phys. Rev. Research **1**, 033102 (2019).
[44] Y.-H. Lu, B.-Z. Wang, and X.-J. Liu, Ideal Weyl semimetal with 3D spin-orbit coupled ultracold quantum gas, arXiv:1911.07169v2.
[45] Z. Wu, L. Zhang, W. Sun, X.-T. Xu, B.-Z. Wang, S.-C. Ji, Y. Deng, S. Chen, X.-J. Liu, and J.-W. Pan, Realization of two-dimensional spin-orbit coupling for Bose-Einstein condensates, Science **354**, 83 (2016).
[46] W. Sun, B.-Z. Wang, X.-T. Xu, C.-R. Yi, L. Zhang, Z. Wu, Y. Deng, X.-J. Liu, S. Chen, and J.-W. Pan, Highly Controllable and Robust 2D Spin-Orbit Coupling for Quantum Gases, Phys. Rev. Lett. **121**, 150401 (2018).
[47] B. Song, L. Zhang, C. He, T. F. J. Poon, E. Hajiyev, S. Zhang, X.-J. Liu, and G.-B. Jo, Observation of symmetry-protected topological band with ultracold fermions, Sci. Adv. **4**, eaao4748 (2018).
[48] B. Song, C. He, S. Niu, L. Zhang, Z. Ren, X.-J. Liu, and G.-B. Jo, Observation of nodal-line semimetal with ultracold fermions in an optical lattice, Nat. Phys. **15**, 911 (2019).
[49] Z.-Y. Wang *et al.*, Realization of ideal Weyl semimetal band in ultracold quantum gas with 3D Spin-Orbit coupling, arXiv:2004.02413.
[50] L. Zhang and X.-J Liu, Spin-orbit coupling and topological phases for ultracold atoms, in *Synthetic Spin-orbit Coupling in Cold Atoms* (World Scientific, Singapore, 2018), Chap. 1, pp. 1–87.
[51] M. Kohmoto, Metal-Insulator Transition and Scaling for Incommensurate Systems, Phys. Rev. Lett. **51**, 1198 (1983).
[52] See the Supplemental Material at http://link.aps.org/supplemental/10.1103/PhysRevLett.125.073204 for details on (i) the finite size scaling analysis, (ii) multifractal analysis, (iii) the case that the incommensurate potential is spin independent, (iv) the topological phase transitions, (v) expansion dynamics, (vi) experimental realization of the present model, and (vii) experimental detection of the noninteracting critical phase, which includes Ref. [3,24,28,34,35,53–56].

[53] Y. Hashimoto, K. Niizeki, and Y. Okabe, A finite-size scaling analysis of the localization properties of one-dimensional quasiperiodic systems, J. Phys. A **25**, 5211 (1992).

[54] W. DeGottardi, D. Sen, and S. Vishveshwara, Topological phases, Majorana modes and quench dynamics in a spin ladder system, New. J. Phys. **13**, 065028 (2011); W. DeGottardi, D. Sen, and S. Vishveshwara, Majorana Fermions in Superconducting 1D Systems Having Periodic, Quasiperiodic, and Disordered Potentials, Phys. Rev. Lett. **110**, 146404 (2013).

[55] J. Zhong, R. B. Diener, D. A. Steck, W. H. Oskay, M. G. Raizen, E. W. Plummer, Z. Zhang, and Q. Niu, Shape of the Quantum Diffusion Front, Phys. Rev. Lett. **86**, 2485 (2001).

[56] T. G. Tiecke, Properties of Potassium, 2011, http://www.tobiastiecke.nl/archive/PotassiumProperties.pdf.

[57] U. Schneider, L. Hackermüller, J. P. Ronzheimer, S. Will, S. Braun, T. Best, I. Bloch, E. Demler, S. Mandt, D. Rasch, and A. Rosch, Fermionic transport and out-of-equilibrium dynamics in a homogeneous Hubbard model with ultracold atoms, Nat. Phys. **8**, 213 (2012).

[58] P. Jurcevic, H. Shen, P. Hauke, C. Maier, T. Brydges, C. Hempel, B. P. Lanyon, M. Heyl, R. Blatt, and C. F. Roots, Direct Observation of Dynamical Quantum Phase Transitions in an Interacting Many-Body System, Phys. Rev. Lett. **119**, 080501 (2017).

[59] In experiment, the spatial configuration of initial and finial states can be measured by quantum gas microscopy (see Ref. [60] for a review). One can approximate the return probability $P(t) \approx N_i/N_z$ after repeating the initialization and measurement by $N_z \gg 1$ number of times, where N_i is the number of times that the final state returns to the initial state at the evolution time t.

[60] H. Ott, Single atom detection in ultracold quantum gases: A review of current progress, Rep. Prog. Phys. **79**, 054401 (2016).

[61] D. J. Luitz, N. Laflorencie, and F. Alet, Many-body localization edge in the random-field Heisenberg chain, Phys. Rev. B **91**, 081103 (2015).

[62] M. Rigol, V. Dunjko, and M. Olshanii, Thermalization and its mechanism for generic isolated quantum systems, Nature (London) **452**, 854 (2008).

[63] The corresponding Hilbert space size for $L = 8$ ($D_H = \binom{16}{4} = 1820$) is not large enough, and the value of η is close to zero near the MBC-to-MBL phase transition.

[64] O. Mandel, M. Greiner, A. Widera, T. Rom, T. W. Hänsch, and I. Bloch, Coherent Transport of Neutral Atoms in Spin-Dependent Optical Lattice Potentials, Phys. Rev. Lett. **91**, 010407 (2003).